Inorganic Chemistry

Article

pubs.acs.org/IC

New Family of Lanthanide-Based Complexes with Different Scorpionate-Type Ligands: A Rare Case Where Dysprosium and Ytterbium Analogues Display Single-Ion-Magnet Behavior

Anthony Lannes and Dominique Luneau*

Laboratoire des Multimatériaux et Interfaces (UMR 5616), Université Claude Bernard Lyon 1, Campus de La Doua, 69622 Cedex Villeurbanne , France

Supporting Information

ABSTRACT: A new family of lanthanide complexes $[Ln(Tpz)_2Bpz]\cdot xCH_2Cl_2$ (Ln = Gd, Tb, Dy, Ho, x = 0.5; Ln = Yb, x = 1; Tpz = hydrotris(pyrazolyl)-borate; Bpz = dihydrobis(pyrazolyl)borate) has been synthesized. Those complexes have been characterized by single-crystal X-ray diffraction, and the magnetic properties have been investigated. Both dysprosium and ytterbium analogues display single-ion-magnet behavior, despite the difference in their spatial distribution of 4f electronic charges. Theoretical calculations with crystal field parameters have been carried out to gain better insight of the relaxation pathways that may be involved in those two complexes.

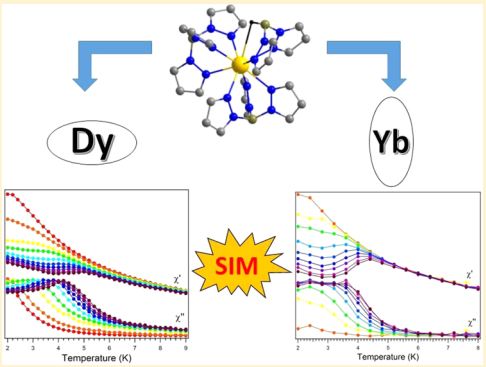

INTRODUCTION

Lanthanides are unique elements for the design of bistable molecular magnetic materials, such as single-molecule magnets (SMMs)[1−8] and single-ion magnets (SIMs).[9−12] This holds that they generally have a large magnetic anisotropy easy axis coming from the unquenched orbital angular momentum of their inner and partially occupied 4f orbitals, combined with the spin−orbit coupling and the ligand field symmetry (LF).[13,14] The latter leads to an energy barrier between the doubled-degenerated $\pm m_J$ magnetic substates of the J ground state and determines the slow relaxation of the magnetization.[15]

The discovery of the first SIM, in a double-decker phthalocyanine complex of terbium(III) (Tb−Pc),[16] led to intense and fruitful research in this field. Similar complexes were designed to place the lanthanide ions in a high-symmetry environment. This was achieved thanks to ligands such as polyoxometallates (POMs),[17,18] cyclopentadienyl (Cp)[19] and its pentamethyl analogue (Cp*),[20] or cyclooctatrienyl (COT).[12] Magnetostructural correlations of the ligand fields have been tried with more or less success to explain the appearance or not of the slow relaxation of magnetization in mononuclear lanthanide complexes.[14] With regard to this, Rinehart and Long have suggested a model giving an easy and reliable way to predict whether a lanthanide complex would be a SIM. It is based on the interaction of the spatial distribution of the 4f electron negative charges with those of the ligand donor atoms.[21] Following, the 4f orbitals can have a spherical geometry (case of Gd(III)), an oblate geometry (elongated, cases of Tb(III) or Dy(III)), or a prolate geometry (flattened, cases of Er(III) or Yb(III)). To observe a magnetic anisotropy easy axis, the ligand field should stabilize the sublevel with the largest projection of the total angular momentum J. This is achieved when the negative charges are concentrated in an axial position for oblate ions and in an equatorial position for the prolate ions. This means that, in a same ligand environment, either the prolate or the oblate geometry will be favored.

Herein we report a new family of isostructural mononuclear lanthanide complexes $[Ln^{III}(Tpz)_2Bpz]$ (Ln = Gd, Tb, Dy, Ho, and Yb) bearing two kinds of scorpionate-type ligands. This family of ligands has already proven to be efficient for the synthesis of SMMs and SIMs.[22−29] In our series, the presence of both ligands, hydrotrispyrazolylborate (Tpz) and dihydrobispyrazolylborate (Bpz), leads to the observation of slow relaxation of the magnetization in both dysprosium and ytterbium analogues. This is quite remarkable considering the preceding explanation since dysprosium(III) has an oblate electron density but ytterbium(III) has a prolate one. Crystal field parameter calculations were performed to try to give an explanation for the relaxation pathways source. Moreover, while SIMs based on dysprosium(III) are now countless, there are only a few examples based on ytterbium(III).[30−33]

EXPERIMENTAL SECTION

Materials. All reactions were carried out in aerobic conditions. All reagents and solvents were purchased from commercial sources and used without further purifications. Potassium hydrotris(pyrazolyl)-borate and potassium dihydrobis(pyrazolyl)borate were synthesized as previously reported.[34]

Received: February 22, 2015
Published: July 1, 2015

DOI: 10.1021/acs.inorgchem.5b00432
Inorg. Chem. 2015, 54, 6736−6743

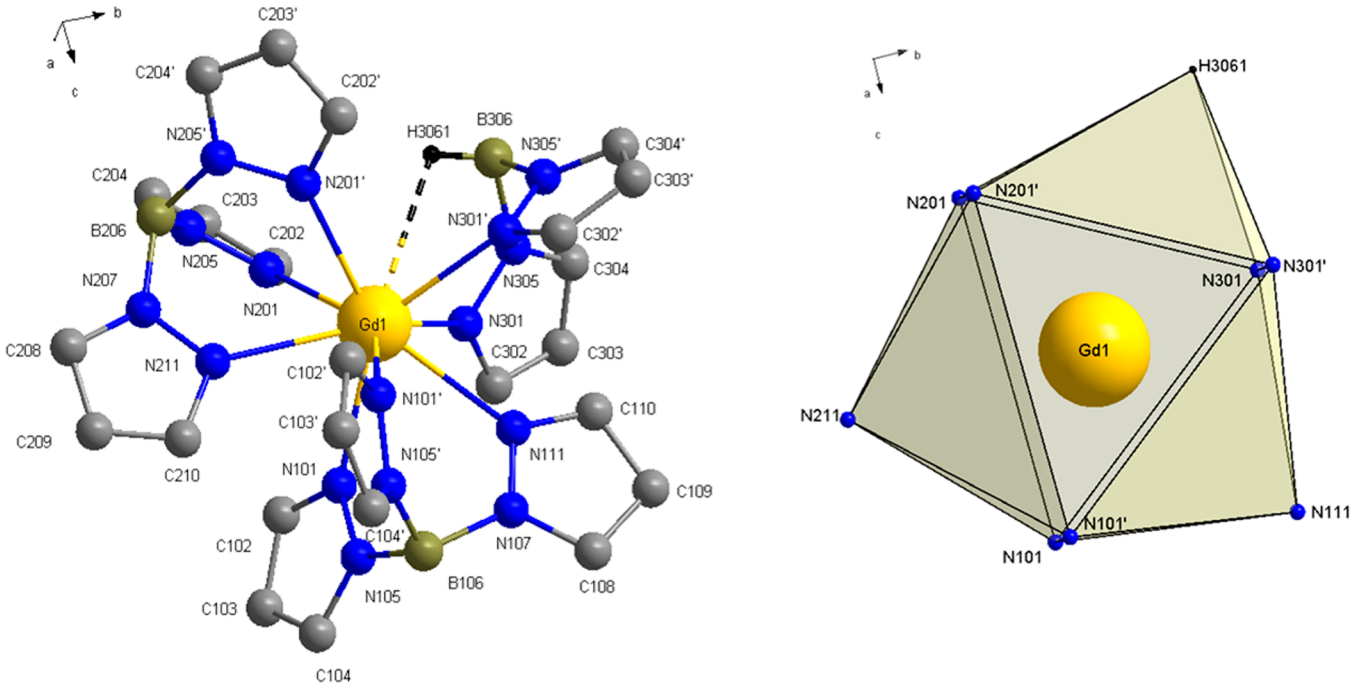

Figure 1. (Left) Structure of **1**. Hydrogen atoms (except capping one) and solvent molecule are omitted for clarity. (Right) Distorted spherical capped square antisprism geometry of the metal center for **1**.

Synthesis of Compounds $[Ln(Tpz)_2Bpz]\cdot xCH_2Cl_2$. Potassium hydrotris(pyrazolyl)borate (100 mg, 0.4 mmol) and potassium dihydrobis(pyrazolyl)borate (37 mg, 0.2 mmol) were dissolved in 15 mL of distillated water. Then to the solution of scorpionate ligand was added under stirring 0.2 mmol of lanthanide chloride hydrate ($GdCl_3\cdot 6H_2O$, 74 mg; $TbCl_3\cdot 6H_2O$, 75 mg; $DyCl_3\cdot 6H_2O$, 75 mg; $HoCl_3\cdot 6H_2O$, 76 mg; $YbCl_3\cdot 6H_2O$, 78 mg) dissolved in 10 mL of distillated water. To the resulting milky solution was then added 40 mL of CH_2Cl_2. The mixture was vigorously stirred for 1 h, and the organic layer was separated. The aqueous layer was then extracted 3 times with 10 mL of CH_2Cl_2. The organic layers were combined, dried over Na_2SO_4, and set in a quiet place for crystallization by slow evaporation. After a week, stick-shaped colorless X-ray quality crystals were collected by filtration. Yield: 65−75%.

Crystal Structure Determination. Single-crystal X-ray studies were carried out using an Xcalibur diffractometer and the related analysis software.[35] An absorption correction based on the crystal faces was applied to the data sets (*analytical*).[36] All structures were solved by direct methods using the SIR97 program[37] combined with Fourier difference syntheses and refined against F using reflections with $[I/s(I) > 3]$ with the CRYSTALS program.[37,38] All atomic displacement parameters for non-hydrogen atoms have been refined with anisotropic terms. The hydrogen atoms were theoretically located on the basis of the conformation of the supporting atom and refined keeping restraints (*riding mode*).

Dichloromethane solvent molecules were refined with occupancy of 0.5 in the case of **1**, **2**, **3**, and **4**, while it was refined with occupancy of 1 for **5**. The refinement did not converge using other values.

Powder X-ray Diffraction. Powder X-ray diffraction (XRD) diagrams were collected on a Siemens D5000 instrument working in transmission mode. It is equipped with an Inel XRG-3000 generator with a copper wavelength λ = 1.54056 Å (Cu Kα_1) and a localization detector. Diagrams were collected overnight between 10° and 70° with 0.032 steps at a speed of 20 s/step. Each diagram has been compared to the calculated one obtained from the single-crystal XRD.

Magnetic Measurements. Magnetic susceptibility data (2−300 K) were collected on powdered polycrystalline samples on a Quantum Design MPMS-XL SQUID magnetometer under an applied magnetic field of 0.1 T, using a sample holder equipped with a piston to prevent orientation with the magnetic field. Alternating current (ac) measurements were performed in the 2−10 K range using a 2.7 G ac field oscillation in 1−1500 Hz range. Magnetization isotherms were collected at 2 K between 0 and 5 T. All data were corrected for the contribution of the sample holder and the diamagnetism of the samples estimated from Pascal's constants.[39]

RESULTS AND DISCUSSION

Crystal Structures. $[Ln(Tpz)_2Bpz]\cdot xCH_2Cl_2$ (Ln = Gd (**1**), Tb (**2**), Dy (**3**), Ho (**4**), x = 0.5; Yb (**5**), x = 1) complexes all crystallize in the $Cmc2_1$ (No. 36) orthorhombic non-centrosymetric space group. Therefore, only the structure of **1** (Gd) will be described. The lattice parameters are a = 13.372(5) Å, b = 17.327(5) Å, c = 14.665(5) Å, and V = 3397.8(2) Å^3. The asymmetric unit of **1** can be described as one Gd(III) ion, two hydrotris(pyrazolyl)borate ligands, one dihydrobis(pyrazolyl)borate ligand, and half a molecule of disordered dichloromethane (Figure 1).

The Gd(III) ion is located on a mirror plane; therefore atoms obtained from this symmetry are denoted with a prime in their label. The Gd(III) is coordinated to eight nitrogens and one hydrogen. Six nitrogen atoms are coming from the two hydrotris(pyrazolyl)borate ligands coordinating by N101, N101′, N111, N201, N201′, and N211 from the pyrazolyl groups and two nitrogen are coming from the dihydrobis-(pyrazolyl)borate ligand coordinating by N301 and N301′ from the pyrazolyl group. The Gd−N bond lengths are in the range of 2.50(1)−2.61(1) Å. The gadolinium metal center is also coordinated to a hydrogen atom H3061, coming from the Bpz ligand.

Previous studies on tris(dihydrobispyrazolylborato)yttrium-(III)[40] $[Y(Bpz)_3]$ and on tris(hydrotrispyrazolylborato)-neodymium(III) and its praseodymium(III) analogue[41] $[Ln(Tpz)_3]$ have shown that the coordination sphere around the metal center was a tricapped trigonal regular prism. It has been demonstrated by ^{89}Y NMR that there exist B−H···Y agostic bonds in $[Y(Bpz)_3]$, allowing a 9-coordinated geometry. While

DOI: 10.1021/acs.inorgchem.5b00432
Inorg. Chem. 2015, 54, 6736−6743

the Y−B average distance is 3.21 Å in $[Y(Bpz)_3]$, it is 3.80 Å for the Nd−B and Pr−B average distances in $[Ln(Tpz)_3]$. In our case, the average distance is 3.65 Å by considering the Gd−B106 and Gd−B206 bond lengths coming from the Tpz ligands. However, the Gd−B306 bond length coming from the Bpz ligand is 3.36(3) Å. It is likely to assume that there is also a B−H···Ln agostic bond in this family of complexes, so that the metal centers are 9-coordinated.

The metal center coordination geometry has been determined by continuous shape measurement via the SHAPE software.[42] All of the values are listed in Table S1 in the Supporting Information. It appears that the geometry in **1** and **2** is closer to the spherical capped square antisprim, while in **3**, **4**, and **5** it is closer to tricapped trigonal regular prism. In **1** and **2** the two twisted faces of the antiprism are made of N111, N301, N301′, and H3061 atoms and N101, N101′, N201, and N201′atoms, the latter being the capped face, where the capping atom is N211. Torsion angles between twisted faces vary from 41.3° to 49.9°. In **3**−**5** (Supporting Information Figures S3−S5) the faces of the trigonal prism are formed by N101, N101′, N201, N201′ and N101, N101′, N301, N301′ and are capped by N211 and N111, respectively, the third face of the prism being capped by the H3061 hydrogen atom. It has to be noticed that the bond lengths of Dy and the capping nitrogen are the longest in the metal center coordination sphere.

The packing of **1** (Figure 2) can be described as isolated $[Gd(Tpz)_2Bpz]$ entities leading to long Gd···Gd distances, and

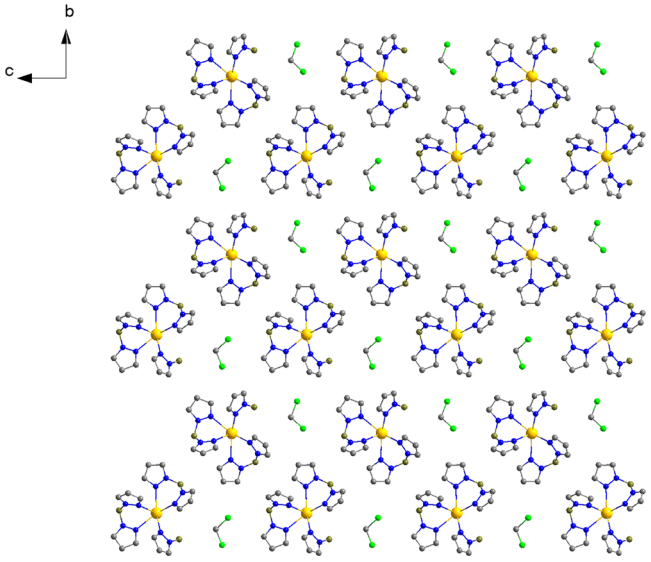

Figure 2. Crystal packing of **1** along the *a* axis. Hydrogen atoms are omitted for clarity.

most likely preventing intermolecular magnetic interactions. The shortest Gd···Gd distance is 9.964(4) Å which is ascribed to significant steric hindrance created by the large Tpz and Bpz ligands.

Crystal data for **1**, **2**, **3**, **4**, and **5** are presented in Table 1. Selected bond lengths and bond angles of metal ions in **1**, **2**, **3**, **4**, and **5** are given in Table 2 and Table 3, respectively. More information is available in CIFs and the Supporting Information.

Magnetic Properties. Magnetic measurements in direct current (dc) and alternating current (ac) modes were recorded at variable temperatures and magnetic fields and performed on all compounds $[Ln(Tpz)_2Bpz]\cdot x CH_2Cl_2$ with Ln = Gd (**1**), Tb (**2**), Dy (**3**), Ho (**4**), and Yb (**5**).

The magnetic susceptibilities of **1**, **2**, **3**, **4**, and **5** (Figure 3a) were recorded between 300 and 2 K in a magnetic field of 1000 Oe. The found χT values at 300 K are 7.74 emu·K·mol^{-1} ($^8S_{7/2}$ and g = 2), 10.91 emu·K·mol^{-1} ($^7F_6$ and g = 3/2,), 14.09 emu·K·mol^{-1} ($^6H_{15/2}$ and g = 4/3), 13.64 emu·K·mol^{-1} ($^5I_8$ and g = 5/4), 2.76 emu·K·mol^{-1} ($^2F_{7/2}$ and g = 8/7), respectively. The values are in good agreement with the expected ones (7.88 emu·K·mol^{-1} for one isolated Gd, 11.8 emu·K·mol^{-1} for one isolated Tb, 14.1 emu·K·mol^{-1} for one isolated Dy, 13.8 emu·K·mol^{-1} for one isolated Ho, and 2.7 emu·K·mol^{-1} for one isolated Yb).

The χT value for **1** remains almost constant all over the temperature range and starts to decrease at 6 K to reach a 6.74 emu·K·mol^{-1} value at 2 K. For **2**, χT slowly decreases to 10.45 emu·K·mol^{-1} at 110 K, then decreases faster to 8.22 emu·K·mol^{-1} at 6 K, and falls to 6.89 emu·K·mol^{-1} at 2 K. For **3**, χT smoothly decreases from 300 to 8 K to reach a 10.50 emu·K·mol^{-1} value, then decreases sharply to 9.05 emu·K·mol^{-1} at 2 K. For **4**, χT continuously decreases from 300 to 70 K to reach a 12.03 emu·K·mol^{-1} value, then falls to reach a 5.40 emu·K·mol^{-1} value at 2 K. For **5**, χT continuously decreases from 300 to 6 K to reach a 1.25 emu·K·mol^{-1} value; then χT decreases to 2 K to reach a value of 0.90 emu·K·mol^{-1}.

The field dependence of **1**, **2**, **3**, **4** and **5** was measured at 2 K in the range field of 0−50 kOe (Figure 3b). Upon increasing the magnetic field, the magnetization of **1**, **2**, **3**, **4** and **5** reaches values of 6.88, 4.61, 5.51, 4.93, and 1.91 μB, respectively. Only the magnetization value for **1** is in agreement with the expected value of 7 μB. All others values are far below the expected values of 8.87, 9.84, 9.82, and 3.80 μB, for **2**, **3**, **4**, and **5**, respectively, and do not saturate. This may indicate the presence of anisotropy and/or low-lying excited states.

The spin dynamics of complexes **2**, **3**, **4**, and **5** have been investigated. Alternating current measurements have been done in the temperature range of 2−9 K at various frequencies. Without application of an external magnetic field, none of the compounds displayed relaxation of magnetization. The application of a static field of 1500 Oe allows the observation of magnetization relaxation in compounds **3** and **5**.

The χ' and χ'' vs T variations are shown in Figures 4 and 5. Both the in-phase (χ') and out-of-phase (χ'') ac susceptibilities are frequency-dependent below 9 K and exhibit maxima values for **3**. The peak temperature of χ'' can be fitted with the Arrhenius law $\tau = \tau_0 \exp[\Delta/(k_B T)]$, where T is the temperature of the χ'' maximum at different frequencies and $\tau = 1/2\pi\nu$, which allows the estimation of the magnetization relaxation parameters. Under an applied magnetic field of 1500 Oe, and by assuming that only an Orbach process occurs in the magnetization relaxation of complex **3**, the preexponential factor is $\tau_0 = 5 \times 10^{-6}$ s and the energy barrier for the relaxation of the magnetization is Δ = 14.09 cm^{-1} with a R factor of 0.9976 (Figure 4), in accordance with the single-ion-magnet behavior. Complex **5** also shows field-induced frequency dependence of its ac susceptibilities (Figure 5), with Δ = 20.11 cm^{-1} (Orbach process only) and $\tau_0 = 2 \times 10^{-8}$ s with R factor of 0.9839, by assuming that magnetization relaxation is due to an Orbach process only.

Those results show two interesting features: the fact that dysprosium and ytterbium derivatives both show SIM properties in the same coordinating environment and the absence of

DOI: 10.1021/acs.inorgchem.5b00432
Inorg. Chem. 2015, 54, 6736−6743

Table 1. Crystal Data for $[Gd(Tpz)_2(Bpz)]\cdot 0.5CH_2Cl_2$ (1), $[Tb(Tpz)_2(Bpz)]\cdot 0.5CH_2Cl_2$ (2), $[Dy(Tpz)_2(Bpz)]\cdot 0.5CH_2Cl_2$ (3), $[Ho(Tpz)_2(Bpz)]\cdot 0.5CH_2Cl_2$ (4), and $[Yb(Tpz)_2(Bpz)]\cdot CH_2Cl_2$ (5)

	1	2	3	4	5
formula	$C_{49}H_{58}B_6Cl_2Gd_2N_{32}$	$C_{49}H_{58}B_6Cl_2N_{32}Tb_2$	$C_{49}H_{58}B_6Cl_2Dy_2N_{32}$	$C_{49}H_{58}B_6Cl_2Ho_2N_{32}$	$C_{25}H_{30}B_6Cl_2N_{16}Yb$
M (g/mol)	1545.53	1548.84	1555.98	1560.84	831.0
cryst shape, color	plate, colorless	stick, colorless	stick, colorless	stick, colorless	stick, colorless
size (mm^3)	0.19 × 0.24 × 0.74	0.15 × 0.17 × 0.81	0.20 × 0.30 × 0.43	0.08 × 0.10 × 0.35	0.17 × 0.23 × 0.28
cryst syst	orthorhombic	orthorhombic	orthorhombic	orthorhombic	orthorhombic
space group (No.)	$Cmc2_1$ (36)	$Cmc2_1$ (36)	$Cmc2_1$ (36)	$Cmc2_1$ (36)	$Cmc2_1$ (36)
T (K)	293	293	293	293	293
λ(Mo Kα) (Å)	0.71073	0.71073	0.71073	0.71073	0.71073
a (Å)	13.372(5)	13.364(5)	13.396(5)	13.442(5)	13.663(5)
b (Å)	17.327(5)	17.328(5)	17.295(5)	17.306(5)	17.178(5)
c (Å)	14.665(5)	14.669(5)	14.667(5)	14.691(5)	14.661(5)
V ($Å^3$)	3397.8(2)	3396.9(2)	3398.1(2)	3417.5(2)	3441.0(2)
Z	2	2	2	2	4
D (g/cm^3)	1.510	1.514	1.521	1.517	1.604
μ (mm^{-1})	2.073	2.203	2.320	2.436	2.917
F(000)	1536	1540	1544	1548	1644
Θ range (deg)	2.8−29.5	2.8−29.3	2.7−29.2	2.8−29.3	2.8−29.2
reflcns					
h	−14 ≤ 18	−16-≤16	−18 ≤ 18	−13 ≤ 18	−14 < 18
k	−14 ≤ 23	−23-≤23	−23 ≤ 20	−16 ≤ 23	−21 < 18
l	−18 ≤ 18	−20-≤19	−19 ≤ 16	−17 ≤ 19	−17 < 18
no. of reflcns	8974	10815	14698	8561	11036
indepen reflcns	7510	3602	6571	4164	3972
no. of params	252	252	252	252	260
R_{int}	0.0960	0.0363	0.0520	0.0565	0.0318
R1[a]	0.0535	0.0297	0.0344	0.0370	0.0304
wR2[b]	0.0510	0.0332	0.0360	0.0429	0.0326
GOF on F^2	1.1051	1.0875	1.1019	1.0926	1.0766
$\Delta\rho_{max}/\Delta\rho_{min}$ ($e\cdot Å^{-3}$)	1.57/−1.33	0.99/−0.42	0.72/−0.62	0.79/−0.58	1.33/−0.51
F[c]	0.00(3)	−0.02(2)	−0.03(2)	−0.01(2)	−0.01(1)

[a] $R1 = \Sigma||F_o| - |F_c||/\Sigma|F_o|$. [b] $wR2 = [\Sigma(w(F_o^2 - F_c^2)^2)/\Sigma(w(F_o^2)^2)]^{1/2}$ with $w = 1/[(\sigma^2F_o^2) + (aP)^2 + bP]$ and $P = (\max(F_o^2) + 2F_c^2)/3$. [c] F = flack parameter.

Table 2. Metal−ligand Bond Length (Å) in 1, 2, 3, 4, and 5

atoms	d (Å)	atoms	d (Å)	atoms	d (Å)	atoms	d (Å)	atoms	d (Å)
Gd−N101	2.501(9)	Tb−N101	2.461 (7)	Dy−N101	2.460(9)	Ho−N101	2.465(9)	Yb−N101	2.428(8)
Gd−N111	2.605(9)	Tb−N111	2.587(5)	Dy−N111	2.598(7)	Ho−N111	2.590(9)	Yb−N111	2.577(7)
Gd−N201	2.526(5)	Tb−N201	2.539(6)	Dy−N201	2.515(9)	Ho−N201	2.499(9)	Yb−N201	2.462(7)
Gd−N211	2.594(8)	Tb−N211	2.575(7)	Dy−N211	2.566(6)	Ho−N211	2.556(6)	Yb−N211	2.556(5)
Gd−N301	2.531(8)	Tb−N301	2.499(4)	Dy−N301	2.481(5)	Ho−N301	2.476(6)	Yb−N301	2.443(5)
Gd−H3061	2.934(3)	Tb−H3061	2.949(2)	Dy−H3061	2.945(2)	Ho−H3061	3.057(2)	Yb−H3061	3.015(2)

Table 3. Bond Angles (deg) in 1, 2, 3, 4, and 5

	angle (deg)				
atoms	Ln = Gd, **1**	Ln = Tb, **2**	Ln = Dy, **3**	Ln = Ho, **4**	Ln = Yb, **5**
N101−Ln−N111	69.0(3)	69.7(1)	69.3(2)	70.2(3)	70.8(2)
N101−Ln−N201	89.2(2)	88.9(2)	88.9(1)	88.3	88.2(1)
N111−Ln−N201	140.8(2)	140.0(1)	140.3(2)	139.7(2)	139.1(1)
N101−Ln−N211	71.1(5)	70.5(2)	71.1(3)	71.5(4)	69.9(3)
N111−Ln−N211	126.7(6)	126.8(3)	126.8(4)	128.6(5)	127.1(3)
N101−Ln−N301	84.4(3)	84.9(2)	84.4(2)	84.8(3)	85.5(2)
N111−Ln−N301	69.9(2)	69.7(1)	70.0(2)	68.8(2)	69.0(2)
N201−Ln−N211	70.3(5)	71.3(2)	71.0(3)	70.2(4)	72.4(2)
N201−Ln−N301	124.1(3)	123.7(1)	123.5(2)	124.1(3)	122.8(2)
N211−Ln−N301	138.1(2)	138.3(1)	138.2(1)	138.6(2)	139.2(1)

DOI: 10.1021/acs.inorgchem.5b00432
Inorg. Chem. 2015, 54, 6736−6743

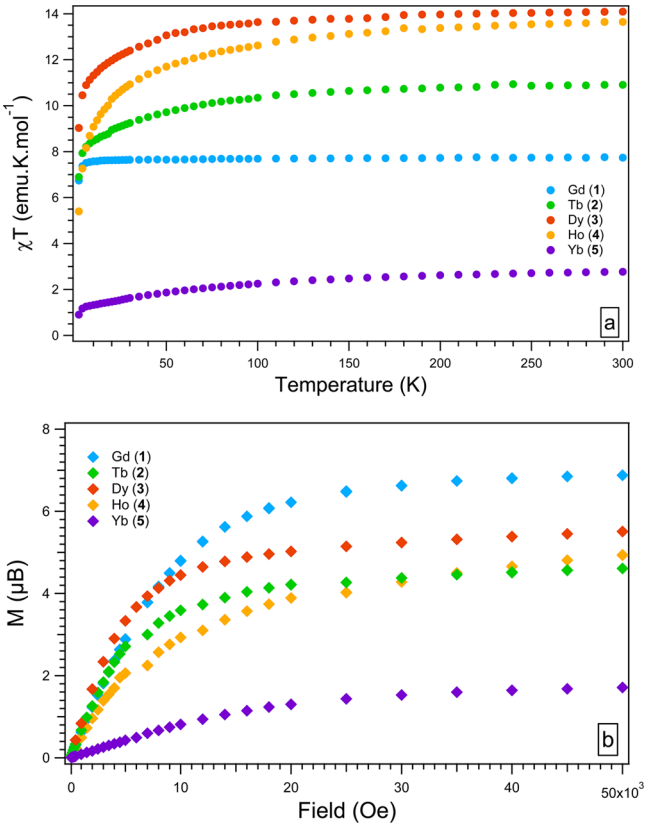

Figure 3. (a) χT vs T plots at 1000 Oe and (b) M vs H plots at 2 K for **1**, **2**, **3**, **4**, and **5**.

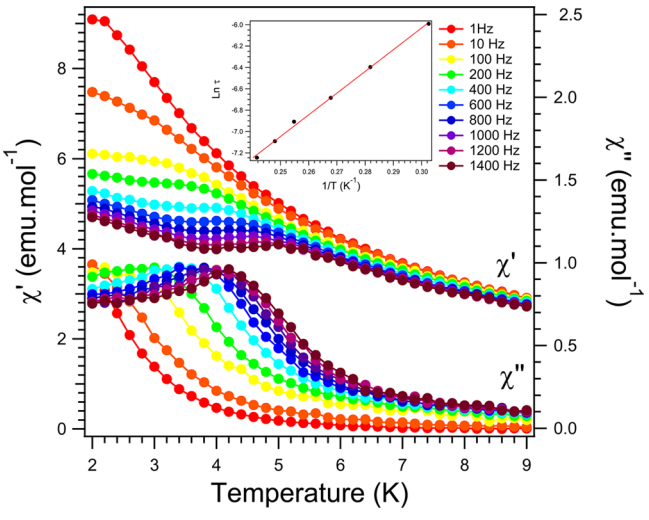

Figure 4. Temperature-dependent in-phase (top) and out-of-phase (bottom) susceptibilities of **3** in a field of 1500 Oe. Lines are eye-guides. Inset: Magnetization relaxation time (τ) vs T^{-1} for **3** in a 1500 Oe field.

SIM properties in terbium analogue, a highly anisotropic Ln(III) ion. This Article aims to understand the first point; the second will be developed in a following work. Indeed, the absence of SIM properties in Tb(III) complexes may be due to several reasons: very fast relaxation processes, the absence of ground state degeneracy (Tb(III) is a non-Kramer ion and is not affected by time-reversal symmetry; thus, the degeneracy is only present with a strict axial symmetry), more studies are needed to determine this origin. To achieve the understanding

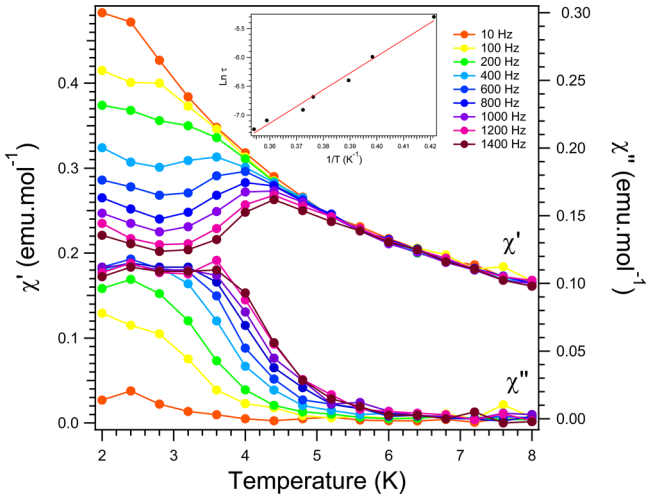

Figure 5. Temperature-dependent in-phase (top) and out-of-phase (bottom) susceptibilities of **5** in a field of 1500 Oe. Lines are eye-guides. Inset: Magnetization relaxation time (τ) vs T^{-1} for **5** at a field of 1500 Oe.

of SIM properties in **3** and **5**, their magnetic susceptibility data have been fitted with a crystal field (CF) Hamiltonian using the PHI program.[43] This Hamiltonian is explained with the following equation:

$$\hat{H}_{CF} = \sum_{n}^{i=1} \sum_{k=2,4,6} \sum_{k}^{q=-k} \sigma_i^k B_{k_i}^q \theta_k \hat{O}_{k_i}^q \qquad \text{(I)}$$

where σ_i^k are the orbital reduction parameters, $B_{k_i}^q$ are the crystal field parameters (CFPs) in Stevens' notation, θ_k are the operator equivalent factors and $\hat{O}_{k_i}^q$ are the operator equivalents. For the tricapped regular trigonal prism of symmetry D_{3h}, the used parameters are $B_2^0, B_4^0, B_6^0 B_6^{-6}$. Of course, the distortion induced by the ligand differences leads to a lower symmetry. In an effort to avoid overparametrization, this lower symmetry was not taken into account, and only the diagonal terms (B_2^0, B_4^0, and B_6^0) and the anisotropic g-factors (g_x, g_y, and g_z) were used to fit the data. Obtained parameters are listed in Table S2 (Supporting Information). The susceptibly fits are shown in Figure 6a and are in very good agreement with the experimental data. With the obtained CFPs, the magnetization data were simulated for both **3** and **5** (Figure 6b), and they are in fair agreement with the experimental data, especially at low fields.

The CFPs make possible the determination of the energy and the composition of substates (listed in Supporting Information Table S3). In an attempt to be as close as possible to the reality, it was specified to the program that magnetic ac susceptibility measurements were carried out under an external magnetic field, a mandatory condition for seeing magnetization relaxation in **3** and **5**. It is known that the application of such a field causes the magnetization relaxation to slow by suppressing quantum tunneling effect caused by ground and excited states' double degeneracy. This explains why the ground and excited states in **3** and **5** are not found doubly degenerated. For both **3** and **5**, all substates are found to be singlet, due to field-induced dissymmetry. The ground substate for **3** is the $|m_J\rangle = -13/2$ state while the $|m_J\rangle = +13/2$ state is only 1.238 cm^{-1} higher. The first excited substate is the $|m_J\rangle = -1/2$ substate at 17.52 cm^{-1}. The energy levels are depicted in Figure 7. The $|m_J\rangle$ =

DOI: 10.1021/acs.inorgchem.5b00432
Inorg. Chem. 2015, 54, 6736−6743

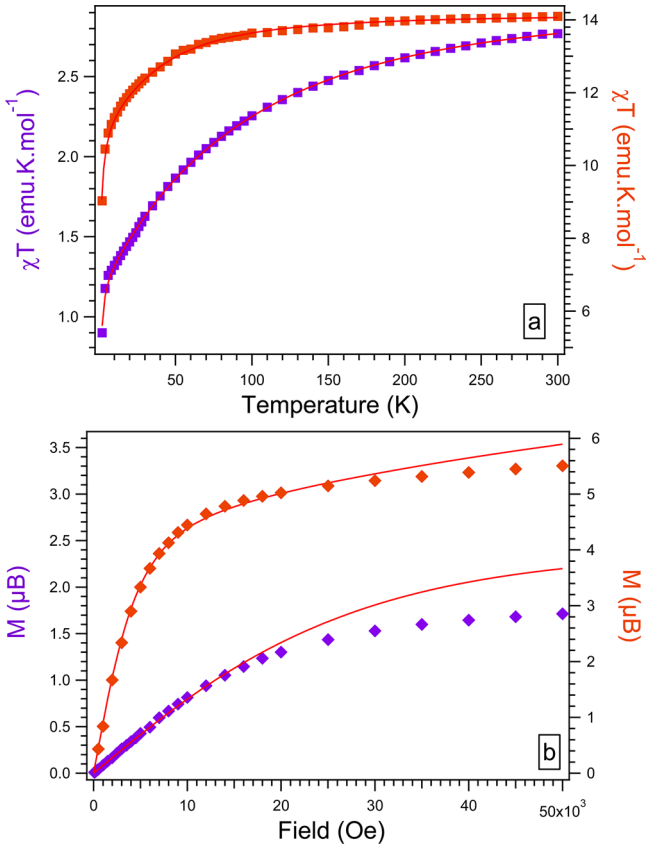

Figure 6. (a) Fits (red lines) of χT vs T plots for **3** and **5**. (b) Simulation (red lines) of M vs H plots for **3** and **5** with the crystal field parameters obtained from fits.

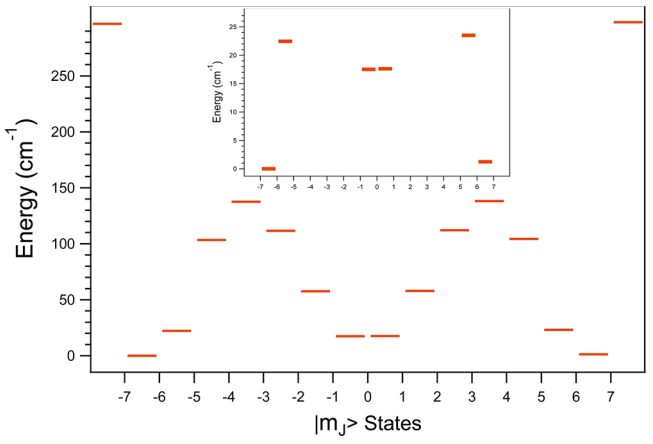

Figure 7. Energy level diagram obtained from the crystal field parameters for **3**. Inset: focus on the 0−30 cm^{-1} part.

+1/2 state is at 17.62 cm^{-1}, giving rise to an excellent relaxation pathway. Because the ±1/2 states are very close in energy, as soon as the −1/2 state is populated from the −13/2 state, the +1/2 state may be populated. From this point, it may relax in the +13/2 state, with a thermally activated energy barrier of ca. 16 cm^{-1}, very close to the Δ calculated with the Arrhenius law. This means that the relaxation of the magnetization is thermally driven in **3**.

The ground state of **5** is the $|m_J\rangle = -5/2$ substate, while the +5/2 state lies 0.297 cm^{-1} above (shown in Figure 8). The first excited state is the $|m_J\rangle = -1/2$ state at 1.667 cm^{-1} with the +1/

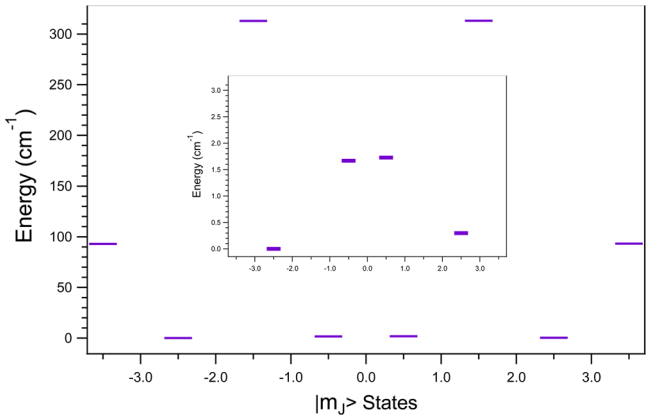

Figure 8. Energy level diagram obtained from the crystal field parameters for **5**. Inset: focus on the 0−3 cm^{-1} part.

2 state at 1.727 cm^{-1}. The ±7/2 states are at ca. 93 cm^{-1}, and the ±3/2 states are at ca. 313 cm^{-1}, far above the others. χ' vs T curves showed a first maximum at 4.5 K before increasing again at lower temperatures. However, none of the energies match the energy barrier Δ calculated from the Arrhenius law, meaning that the Orbach process is not the proper one observed around 4 K, though χ' vs T curves showed there was a maximum at 4.5 K before increasing again at lower temperature, which is likely the sign of two different relaxation processes. Because the measurements were done under an external magnetic field, it is likely that QTM is not present as a relaxation process. Moreover the χ'' vs T curves observed at 1000 Hz with several static fields (Supporting Information Figure S5) show a peak at 3.6 K whose maximum does not vary with increasing magnetic field. This indicates there is no direct process (which would imply a shift at high field) in the magnetization relaxation. What is therefore conceivable is that there is a relaxation pathway via Orbach process at low temperature, with a very small energy barrier Δ, close to the 1−2 cm^{-1} as found in the calculation, while the process at higher temperature is a Raman process. Thus, the energy barrier calculated with the Arrhenius law has no physical meaning and only is an artifact.

The recent result on complexes $[Ln(N(Si(Me)_3)_2]$ (Ln = Dy, Er) has shown how the model by Rinehart and Long works well.[44] These complexes show a nearly perfect planar trigonal geometry, making the prolate electronic shape more favorable to observe SIM properties. Consequently, low reversal of the magnetization was not observed for the dysprosium analogue but for the erbium congener. Interestingly the SIM properties were inverted by adding THF molecules in the coordination sphere to give a near trigonal bipyramid geometry and to favor the oblate electronic shape. In our case, the trigonal prism will most likely favor the oblate electronic shape. However, the presence of capping donor atoms on every face of the prism probably favors the prolate electronic shape, giving rise to an intermediate geometry, where high $|m_J|$ are stabilized for both oblate and prolate electronic shapes. Thus, magnetic anisotropy arises in both cases, and magnetization relaxation may happen. Though relaxation pathways are likely not the same in **3** and **5**, further investigations need to be undertaken to elucidate these fascinating phenomena.

DOI: 10.1021/acs.inorgchem.5b00432
Inorg. Chem. 2015, 54, 6736−6743

CONCLUSION

To summarize, a new family of five complexes in which a lanthanide ion is coordinated by two different scorpionate-type ligands has been synthesized. Their crystallographic structure has been determined and reveals that the compounds are isomorphous, with a metal geometry being distorted capped square antiprism for **1** and **2** and distorted tricapped regular trigonal prismatic for complexes **3**, **4**, and **5**. Their magnetic properties have been investigated and show that compounds **3** and **5** display field-induced single-ion-magnet behavior, thus demonstrating that dysprosium(III) and ytterbium(III) can behave as single-ion magnets in the same coordination environment. At first glance, this may seem surprising. Indeed, since Dy(III) is a prolate ion and Yb(III) an oblate ion, they should not relax when in the same environment. Trying to understand why, theoretical calculation with crystal field parameters were done for the magnetic susceptibility. The extraction of the energy diagram gives a rational explanation. While the relaxation of the magnetization is most likely due to an Orbach process in the dysprosium analogue, it comes from a different process, most likely Raman, in the ytterbium complex. This shows how important metal center geometry and relaxation pathways are to understanding and elaborating on single-molecule and single-ion magnets.

ASSOCIATED CONTENT

Supporting Information

Structures of compounds **2**, **3**, **4**, and **5** (Figures S1−S4, respectively), the 1000 Hz out-of-phase signal at variable magnetic field for compound **5** (Figure S5), calculated and experimental X-ray powder diffraction patterns for **1**−**5** (Figures S6−S10), calculated values with SHAPE software for 9-coordinated geometry (Table S1), calculated crystal field parameters (Table S2) and substates and their corresponding energy levels (Table S3) for compounds **3** and **5**, and crystallographic data in CIF format. The Supporting Information is available free of charge on the ACS Publications website at DOI: 10.1021/acs.inorgchem.5b00432.

AUTHOR INFORMATION

Corresponding Author

*E-mail: luneau@univ-lyon1.fr. Fax: +33 4 72 43 11 60. Tel.: +33 4 72 43 14 18.

Notes

The authors declare no competing financial interest.

ACKNOWLEDGMENTS

A.L. held a CMIRA Explora' doc 2012 fellowship from la Région Rhône-Alpes.

REFERENCES

(1) Guo, Y.-N.; Ungur, L.; Granroth, G. E.; Powell, A. K.; Wu, C.; Nagler, S. E.; Tang, J.; Chibotaru, L. F.; Cui, D. *Sci. Rep.* **2014**, *4*, No. 5471.

(2) Guo, Y.-N.; Xu, G.-F.; Wernsdorfer, W.; Ungur, L.; Guo, Y.; Tang, J.; Zhang, H.-J.; Chibotaru, L. F.; Powell, A. K. *J. Am. Chem. Soc.* **2011**, *133*, 11948−11951.

(3) Guo, Y.-N.; Xu, G.-F.; Gamez, P.; Zhao, L.; Lin, S.-Y.; Deng, R.; Tang, J.; Zhang, H.-J. *J. Am. Chem. Soc.* **2010**, *132*, 8538−8539.

(4) Blagg, R. J.; Muryn, C. A.; McInnes, E. J. L.; Tuna, F.; Winpenny, R. E. P. *Angew. Chem., Int. Ed.* **2011**, *50*, 6530−6533.

(5) Hewitt, I. J.; Tang, J.; Madhu, N. T.; Anson, C. E.; Lan, Y.; Luzon, J.; Etienne, M.; Sessoli, R.; Powell, A. K. *Angew. Chem., Int. Ed.* **2010**, *49*, 6352−6356.

(6) Lin, P.-H.; Burchell, T. J.; Ungur, L.; Chibotaru, L. F.; Wernsdorfer, W.; Murugesu, M. *Angew. Chem., Int. Ed.* **2009**, *48*, 9489−9492.

(7) Lin, S.-Y.; Wernsdorfer, W.; Ungur, L.; Powell, A. K.; Guo, Y.-N.; Tang, J.; Zhao, L.; Chibotaru, L. F.; Zhang, H.-J. *Angew. Chem., Int. Ed.* **2012**, *51*, 12767−12771.

(8) Long, J.; Habib, F.; Lin, P.-H.; Korobkov, I.; Enright, G.; Ungur, L.; Wernsdorfer, W.; Chibotaru, L. F.; Murugesu, M. *J. Am. Chem. Soc.* **2011**, *133*, 5319−5328.

(9) Le Roy, J. J.; Korobkov, I.; Murugesu, M. *Chem. Commun. (Cambridge, U. K.)* **2014**, *50*, 1602−1604.

(10) Branzoli, F.; Carretta, P.; Filibian, M.; Zoppellaro, G.; Graf, M. J.; Galan-Mascaros, J. R.; Fuhr, O.; Brink, S.; Ruben, M. *J. Am. Chem. Soc.* **2009**, *131*, 4387−4396.

(11) Jeletic, M.; Lin, P.-H.; Le Roy, J. J.; Korobkov, I.; Gorelsky, S. I.; Murugesu, M. *J. Am. Chem. Soc.* **2011**, *133*, 19286−19289.

(12) Jiang, S.-D.; Wang, B.-W.; Sun, H.-L.; Wang, Z.-M.; Gao, S. *J. Am. Chem. Soc.* **2011**, *133*, 4730−4733.

(13) Benelli, C.; Gatteschi, D. *Chem. Rev.* **2002**, *102*, 2369−2388.

(14) Sorace, L.; Benelli, C.; Gatteschi, D. *Chem. Soc. Rev.* **2011**, *40*, 3092−3104.

(15) Gatteschi, D. R.; Sessoli, R.; Villain, J. *Molecular Nanomagnets*; Oxford University Press: Oxford, U.K., 2006.

(16) Ishikawa, N.; Sugita, M.; Ishikawa, T.; Koshihara, S.; Kaizu, Y. *J. Am. Chem. Soc.* **2003**, *125*, 8694−8695.

(17) AlDamen, M. A.; Cardona-Serra, S.; Clemente-Juan, J. M.; Coronado, E.; Gaita-Arino, A.; Marti-Gastaldo, C.; Luis, F.; Montero, O. *Inorg. Chem.* **2009**, *48*, 3467−3479.

(18) AlDamen, M. A.; Clemente-Juan, J. M.; Coronado, E.; Marti-Gastaldo, C.; Gaita-Arino, A. *J. Am. Chem. Soc.* **2008**, *130*, 8874−8875.

(19) Sulway, S. A.; Layfield, R. A.; Tuna, F.; Wernsdorfer, W.; Winpenny, R. E. P. *Chem. Commun. (Cambridge, U. K.)* **2012**, *48*, 1508−1510.

(20) Demir, S.; Zadrozny, J. M.; Long, J. R. *Chem.—Eur. J.* **2014**, *20*, 9524−9529.

(21) Rinehart, J. D.; Long, J. R. *Chem. Sci.* **2011**, *2*, 2078−2085.

(22) Zhang, Y.-Z.; Mallik, U. P.; Clérac, R.; Rath, N. P.; Holmes, S. M. *Polyhedron* **2013**, *52*, 115−121.

(23) Zhang, Y.-Z.; Mallik, U. P.; Rath, N. P.; Clérac, R.; Holmes, S. M. *Inorg. Chem.* **2011**, *50*, 10537−10539.

(24) Zhang, Y.-Z.; Mallik, U. P.; Clerac, R.; Rath, N. P.; Holmes, S. M. *Chem. Commun. (Cambridge, U. K.)* **2011**, *47*, 7194−7196.

(25) Li, D.; Clérac, R.; Parkin, S.; Wang, G.; Yee, G. T.; Holmes, S. M. *Inorg. Chem.* **2006**, *45*, 5251−5253.

(26) Jiang, L.; Choi, H. J.; Feng, X.-L.; Lu, T.-B.; Long, J. R. *Inorg. Chem.* **2007**, *46*, 2181−2186.

(27) Bartlett, B. M.; Harris, T. D.; DeGroot, M. W.; Long, J. R. *Z. Anorg. Allg. Chem.* **2007**, *633*, 2380−2385.

(28) Rinehart, J. D.; Long, J. R. *Dalton Trans.* **2012**, *41*, 13572−13574.

(29) Xu, G.-F.; Wang, Q.-L.; Gamez, P.; Ma, Y.; Clerac, R.; Tang, J.; Yan, S.-P.; Cheng, P.; Liao, D.-Z. *Chem. Commun. (Cambridge, U. K.)* **2010**, *46*, 1506−1508.

(30) AlDamen, M. A.; Cardona-Serra, S.; Clemente-Juan, J. M.; Coronado, E.; Gaita-Ariño, A.; Martí-Gastaldo, C.; Luis, F.; Montero, O. *Inorg. Chem.* **2009**, *48*, 3467−3479.

(31) Liu, J.-L.; Yuan, K.; Leng, J.-D.; Ungur, L.; Wernsdorfer, W.; Guo, F.-S.; Chibotaru, L. F.; Tong, M.-L. *Inorg. Chem.* **2012**, *51*, 8538−8544.

(32) Pointillart, F.; Guennic, B. L.; Golhen, S.; Cador, O.; Maury, O.; Ouahab, L. *Chem. Commun. (Cambridge, U. K.)* **2013**, *49*, 615−617.

(33) Sugita, M.; Ishikawa, N.; Ishikawa, T.; Koshihara, S.; Kaizu, Y. *Inorg. Chem.* **2006**, *45*, 1299−1304.

(34) Trofimenko, S. *J. Am. Chem. Soc.* **1967**, *89*, 3170−3177.

(35) *CrysAlisPro*, ODL, Version 1.171.33.46 (release Aug. 27, 2009 CrysAlis171.NET); Agilent Technologies: Oxford, U.K., 2009.

DOI: 10.1021/acs.inorgchem.5b00432
Inorg. Chem. 2015, 54, 6736−6743

(36) De Meulenaar, J.; Tompa, H. *Acta Crystallogr.* **1965**, *19*, 1014−1018.
(37) Cascarano, G.; Altomare, A.; Giacovazzo, C.; Guagliardi, A.; Moliterni, A. G. G.; Siliqi, D.; Burla, M. C.; Polidori, G.; Camalli, M. *Acta Crystallogr.* **1996**, *A52*, C−79.
(38) Watkin, D. J.; Prout, C. K.; Carruthers, J. R.; Betteridge, P. W. *CRYSTALS*, Issue 11; Chemical Crystallography Laboratory: Oxford, U.K., 1999.
(39) Pascal, P. *Ann. Chim. Phys.* **1910**, *19*, 5−70.
(40) Reger, D. L.; Lindeman, J. A.; Lebioda, L. *Inorg. Chem.* **1988**, *27*, 1890−1896.
(41) Apostolidis, C.; Rebizant, J.; Kanellakopulos, B.; von Ammon, R.; Dornberger, E.; Müller, J.; Powietzka, B.; Nuber, B. *Polyhedron* **1997**, *16*, 1057−1068.
(42) Llunell, M.; Casanova, D.; Cirera, J.; Alemany, P.; Alvarez, S. *SHAPE*, v2.1; University of Barcelona and The Hebrew University of Jerusalem: Barcelona and Jerusalem, 2013.
(43) Chilton, N. F.; Anderson, R. P.; Turner, L. D.; Soncini, A.; Murray, K. S. *J. Comput. Chem.* **2013**, *34*, 1164−1175.
(44) Zhang, P.; Zhang, L.; Wang, C.; Xue, S.; Lin, S.-Y.; Tang, J. *J. Am. Chem. Soc.* **2014**, *136*, 4484−4487.

DOI: 10.1021/acs.inorgchem.5b00432
Inorg. Chem. 2015, 54, 6736−6743